TERA PROJECTS IN MEDICAL DIAGNOSTICS
FABIO SAULI (CERN)

CONTRIBUTION TO TERA SILVER BOOK 2023

FOREWORD

My association with TERA started after a discussion with Ugo Amaldi, when we agreed that in parallel with the intense activity of the Foundation on ion accelerators and therapy, it would be desirable to start a research project on patient monitoring and treatment quality. Proposed to the TERA Technical Scientific Committee (CTS) in November 2006, the project AQUA (Advanced Quality Assessment) was approved and budgeted shortly after, under my leadership. Set up in the TERA CERN building 182, the laboratory was equipped with basic instrumentation and hosted the various detector development projects described below. The group was associated to the European Seventh Framework Programs, namely ENLIGHT (European Network for Light Ions Therapy) and ENVISION (European NoVel Imaging Systems for ION therapy), coordinated by Manjit Dosanjh. The AQUA project advances were presented at regular collaboration meetings: CERN (2008, 2009, 2012), Madrid (2009), Lyon (2011), Ciudad Real (2012), Valencia (2013), Roma (2015).
Short- and medium-term collaborators were associated with the group and contributed to the developments described below. They are summarized in Chapter 7.
The AQUA program was completed by the end of 2017. The major outcomes of the research are documented in eight publications in major Journals, three PhD thesis (see references) and many presentations at international conferences and meetings.
My warmest appreciation to Ugo Amaldi for the continuing help and encouragement all along the course of the project.

1. INTRODUCTION

Aiming at research in the field of medical diagnostics within TERA, the project AQUA (Advanced Quality Assessment) was initiated in 2006 and pursued its activity until 2018. Under the leadership of the writer, and in collaboration with other members of the Foundation, the group was staffed by several young fellows with the ambition to study promising solutions for in-beam patient dose monitoring complementing the development efforts towards the design and realization of dedicated accelerator systems and patient monitoring for hadrotherapy, in the framework of the European Network for Light Ion Therapy ("ENLIGHT," 2020) (Dosanjh, 2017).
Four basic technologies have been investigated by the AQUA group, described in the following sections: Depth-of-Interaction (DOI) determination in crystals; Time-of-Flight determination for Positron Emission Tomography (TOF-PET); Proton Range Radiography (PRR) system; Prompt Gamma Monitor (PGM).
Figure 1 is a view of the AQUA laboratory during the development of the PRR1 system.

2. DEPTH-OF-INTERACTION DETERMINATION IN CRYSTAL SCINTILLATORS

A method envisaged for dose monitoring in hadrotherapy relies on the detection of the two collinear 511 keV gamma rays resulting from the beta decay of positron-emitting isotopes created by the beam-target interactions, namely ^{15}O, ^{11}C and ^{13}N. Due to the short lifetime of these isotope (a few to a few tens of minutes) the PET image must be acquired during or immediately after the exposure, implying serious problems of background and accidental counts, that can be moderated exploiting a measurement of the Time-of-Flight (TOF) between the two arms in coincidence. Moreover, to free the space for the beam ports, the standard ring geometry of the PET scanners must have an open geometry, with two facing half-rings, Figure 2.
The effect of the open-ring geometry on the image reconstruction has been analyzed by the AQUA team in collaboration with researchers from Ghent, Dresden and Valencia Universities, using simulation programs (Diblen et al., 2012). Figure 3 is an example of computed spatial resolution as a function of time-of-flight for a full and open ring PET.

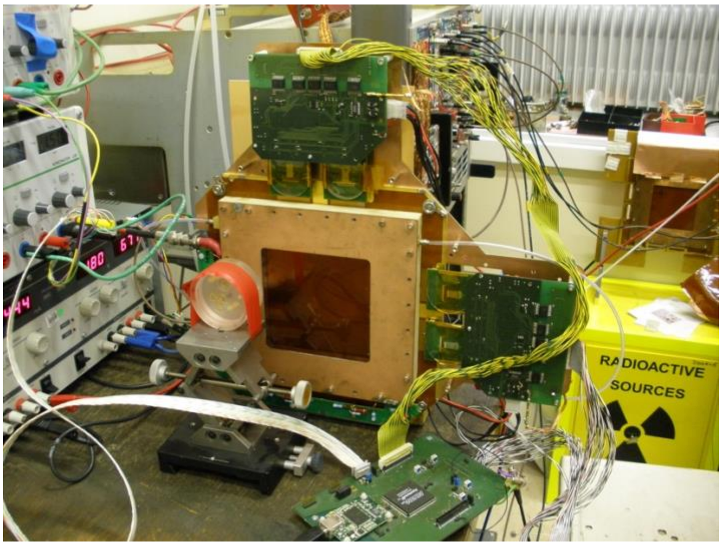

Figure *1*: View of the TERA-AQUA laboratory during the development of the Proton Range Radiography system.

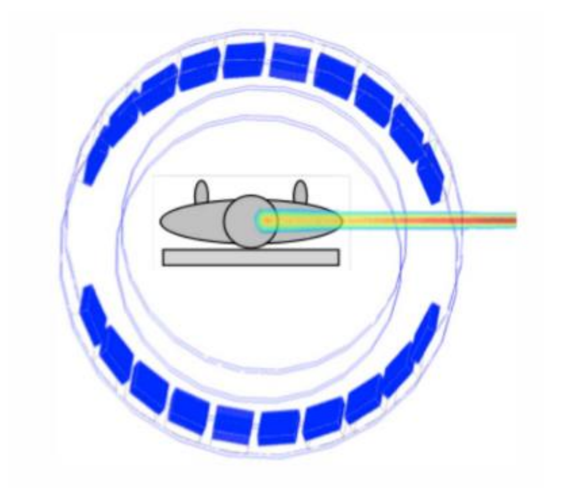

Figure 2: Open PET geometry to allow the beam ports.

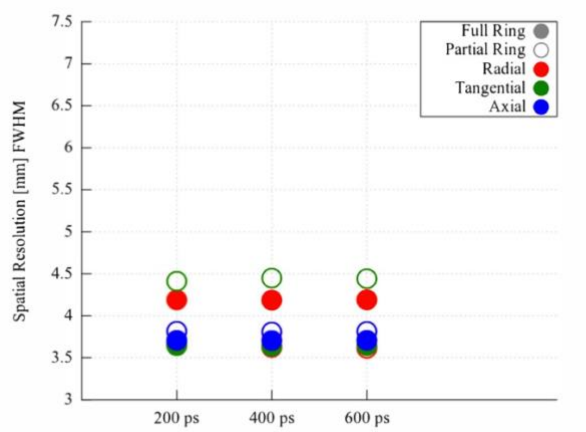

. Figure 3: Simulated space resolution of full and open ring PET as a function of TOF.

It appeared that one dispersive source is the parallax error in positioning the gamma conversion in thick crystals, due to the penetration depth for gammas at angles with the longitudinal direction of the scintillator. This error can be reduced exploiting a method to determine the Depth-of-Interaction (DOI) by recoding the two-dimensional profile of the scintillation photons with a segmented multi-anode photomultiplier (MAPM) sensor, coupled to a thick scintillating crystal (see Figure 4). As shown schematically in the figure, the center-of gravity of the recorded distribution provides the position of the conversion, while its width depends on the distance of the interaction from the sensor.
A multi anode photomultiplier was used to verify experimentally the position and DOI determination accuracies for 511 keV photons. Essential to this extent, the linearity of response was studied with a flood illumination of the sensor, comparing the performance of several commercially available MAPMs. Figure 5 shows the result for a Burle Micro-Channel-Plate tube (MCP-PM), having anode pads and an area of 5x5 cm^2. The 10% variation of efficiency found over the sensitive area is quite adequate for this work.
The expected performances of the DOI determination were studied with the Monte-Carlo optical transport program LITRANI and different choices of scintillating crystals geometries (Solevi, 2007). The best result is obtained using crystals with non-reflective walls (black painted). The simulation predicts a localization accuracy in the DOI Z-direction between one and two mm rms, in fact not attained by the experimental measurements (see below).

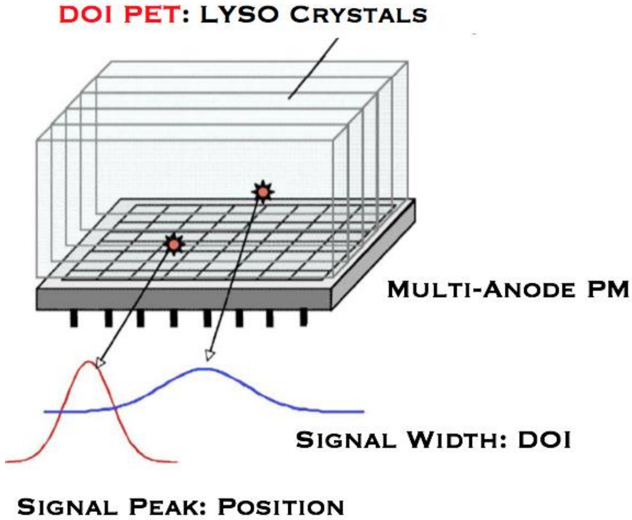

Figure 4: Depth-of-Interaction determination in composite crystal scintillator.

The setup used to determine experimentally the position accuracy is shown in Figure 6. A 10 cm long, 50 mm high scintillating LYSO[1] crystal is mounted in contact with the PM, covering two anode pad rows; a positron-emitting ^{22}Na mounted near the crystal emits a 511 keV gamma, and a collimated BGO crystal provides the coincidence signal on the second photon. Signals are recorded on the anode pads facing the crystal. Figure 7 shows the correlation between the source position and the one computed from the center-of-gravity of the recorded signals. The correlation is linear with a dispersion of 1.2 mm rms, providing the localization accuracy in the plane of the sensor.

An example of the scintillation light distribution for two positions of the source, 27 and 2 mm from the sensor is shown in Figure 8. A fit to the distributions provides a DOI accuracy of around 10 mm, compared to the 50 mm length of the crystal; this is worse than the estimation from the simulation, and is attributed to poorly estimated internal reflections in the crystal.

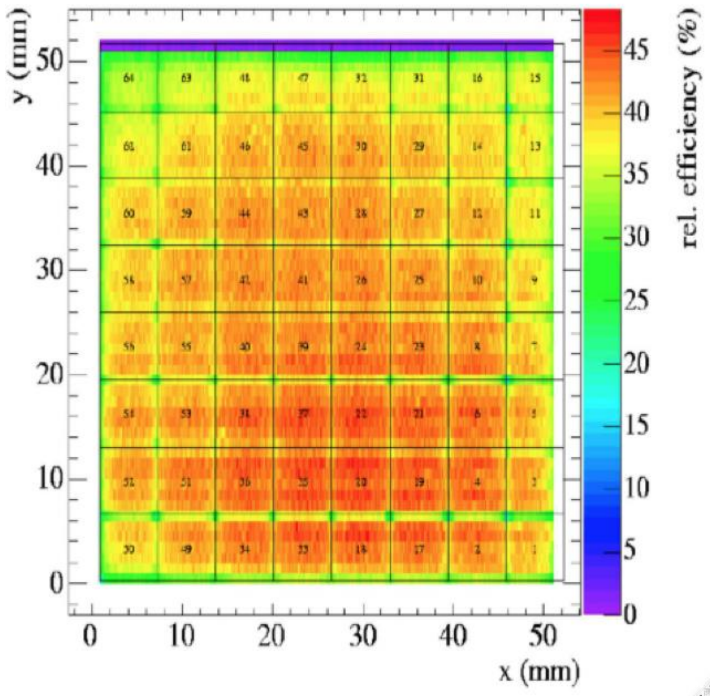

Figure 5: Response uniformity of the 64-anode Burle Micro-Channel-Plate PM

[1] Lutetium Yttrium Oxyorthosilicate

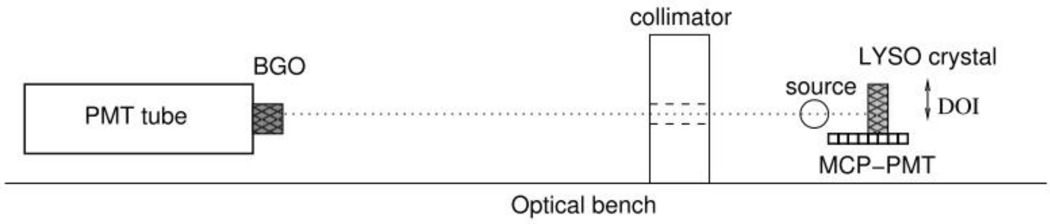

Figure 6: Experimental setup to detect the two collinear 511 keV photons emitted by the ^{22}Na source. The position and DOI can be varied moving the sensor.

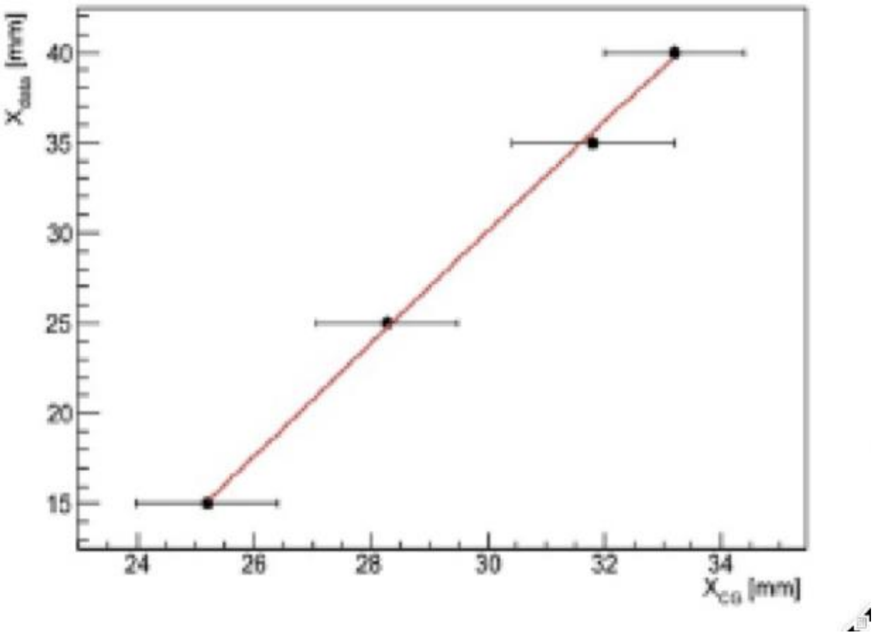

Figure 7: Correlation between the real collimated source position and the one reconstructed from the center-of-gravity of the pulsed recorded on the MCP-PM anodes rows.

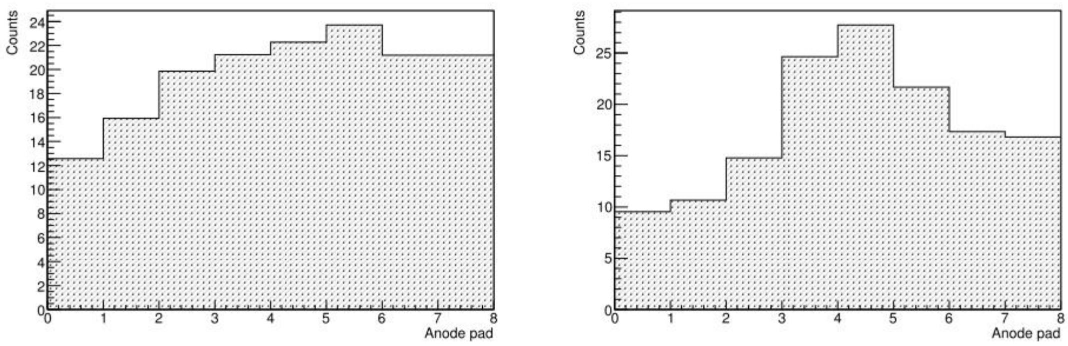

Figure 8: Detected scintillation profile for two depths of conversion in the crystal, 25 mm apart.

3. TIME-OF-FLIGHT PET

An effective way to improve the background rejection in PET detectors is to impose a strict limit in the time difference between the signals produced by the two arms of the detector arrays, the so-called Time-of-Flight PET (TOF-PET). The effect on the image quality of a stopping beam in a water target as a function of the TOF resolution is shown in the simulation of Figure 9 for a crystal-based detector and for the Resistive Plate Detector to be described in what follows (Solevi, 2007).

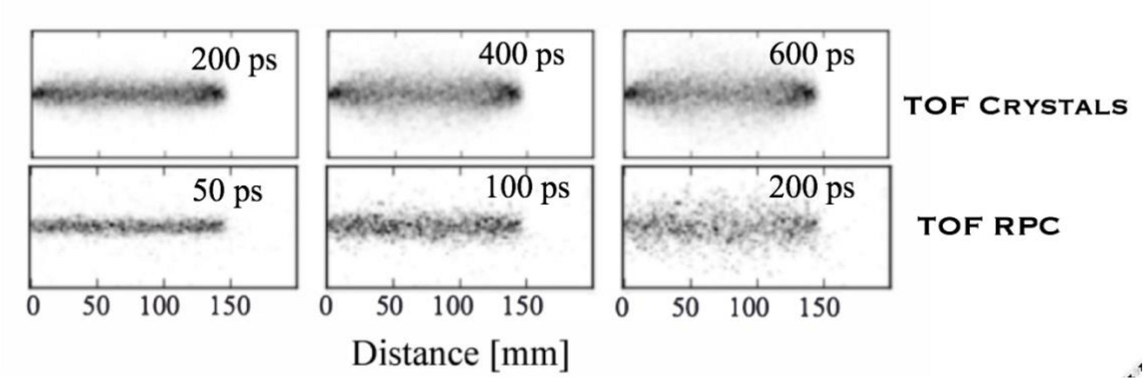

Figure 9: Computed PET image quality of a stopping proton beam for a range of values of the time-of-flight resolution.

Due to their rather long fluorescence decay time, typically 20-40 ns, crystal scintillators do not provide time resolutions below one ns. The Multigap Resistive Plate Chamber (MRPC) (Cerron-Zeballos et al., 1996), a gaseous detector developed for the requirements of particle physics, permits one to achieve TOF resolutions of 50 ps or better in the detection of fast charged particles (Akindinov et al., 2004). This goal is reached using very thin gaseous layers, typically 100 µm, between two high-resistivity glass cathodes operated in the avalanche mode. The low efficiency of ionizing interactions in individual layers is compensated by using stacks of many layers, read-out by a common pickup electrode.

For gamma rays, detection is not achieved by direct ionization of the gas, but by the ionization yields of electrons released by a photoelectric or Compton interaction in the thin glass cathodes. For soda-lime glass, the optimum thickness for detection is around 200 µm, with an efficiency of 0.22%; thicker layers result in self-absorption of the yields. In order to ensure an exploitable efficiency for an MRPC-based TOF device, a stack of several tens of modules has to be implemented (Figure 10), encouraging the development a cheap and reliable design for the detector as described below.

The structure of a 4-gap MGRPC prototype developed by the AQUA group is shown in Figure 11 and Figure 12 (Watts et al., 2013)(Amaldi et al., 2015). Tiny, regularly spaced insulating pillars, grown on the glass plates with photolithography processing ensure the gap thickness on assembly the modules (see Figure 13). Figure 13 shows an assembled prototype with signal pick-up strips read out from the two sides. Colloidal graphite resistive layers in a range between 100 kΩ/square and 1 MΩ/square were deposited on the glass surface. To record the signals, we used the very fast NINO ASIC chip developed by the ALICE MG-RPC group (Anghinolfi et al., 2004).

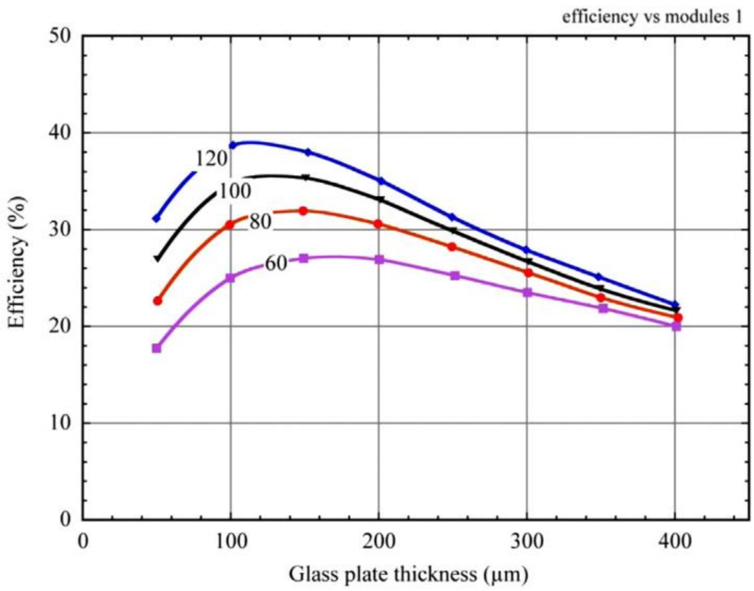

(Figure 10: Computed detection efficiency of 511 keV photons as a function of glass converter thickness and number of 4-gap RPC modules.

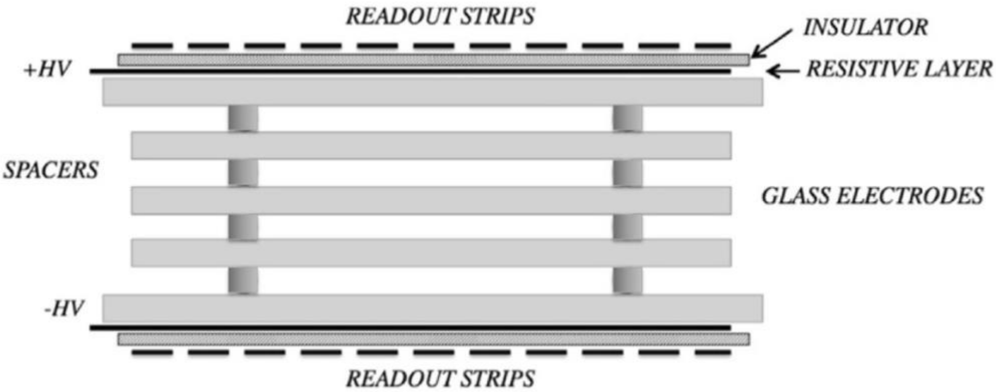

Figure 11: Schematics of a 4-gap MGRPC optimized for 511 keV photons detection.

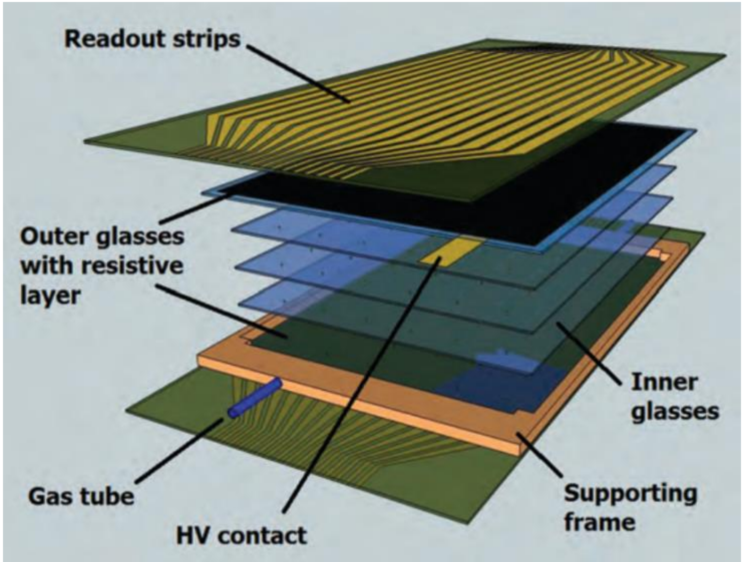

Figure 12: Exploded view of a 4-gap MGRPC AQUA prototype.

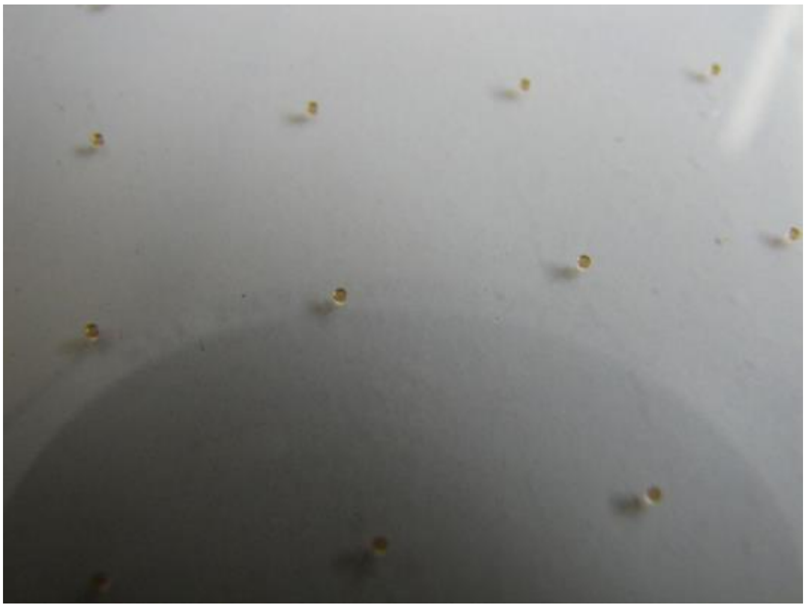
Figure : Gap-restoring insulating pillars, 300 µm wide and 10 mm apart.

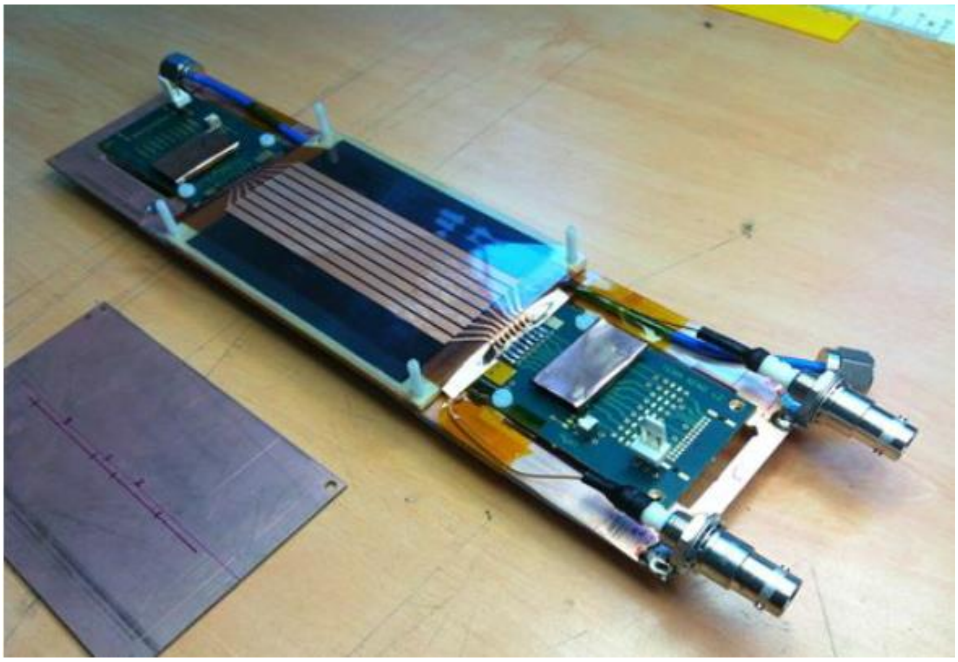

13). Figure 13: Assembled MGRPC prototype, with an active area of 90x65 mm^2 and two-side strips readout.

To measure the TOF resolution, two identical modules were mounted at about 50 cm distance, with the positron-emitting ^{22}Na source in the middle. The efficiency and resolution were deduced from the signals recorded on the two detectors. An example of detection efficiency as a function of applied voltage is given in Figure 14 for a single and a four-gap module and for two choices of the surface resistivity of the coated glass. The experimental efficiency corresponds well to the computed values for the same geometry (Watts, 2014).

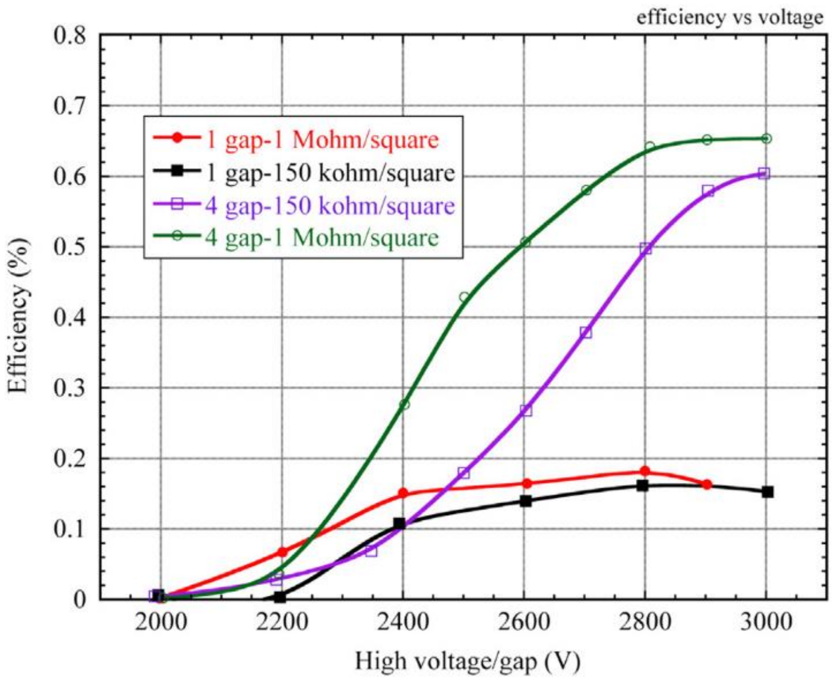

Figure 14: Experimental values of detection efficiency of 511 keV photons for single and multi-gap detectors having different surface resistivity.

The time resolution of the detector, deduced from the time difference between pulses detected on the two sides of the 10 cm long strips, is about 38 ps as shown in Figure 15.
The scatter plot in Figure 16 illustrates the capability of the MGRPC in localizing a collimated gamma source; the source width is 2 mm.

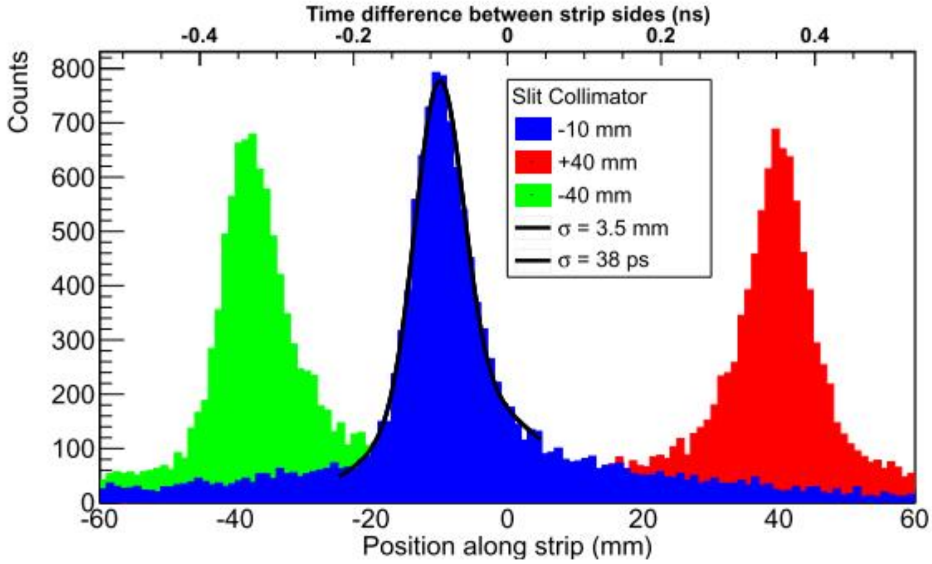

Figure 15: Plots of the time difference between the two sides of the 10 cm long pickup strips of the detector, for different positions of the collimated source.

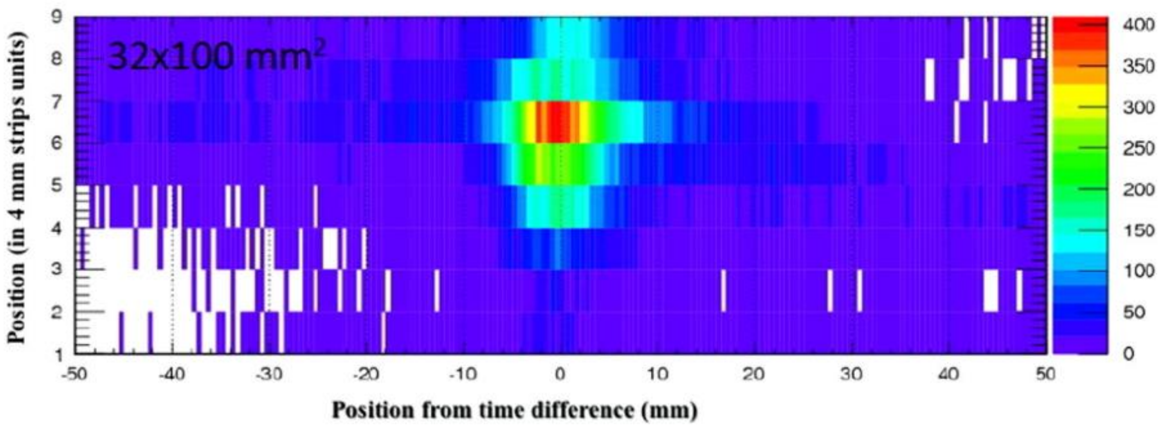

Figure 16: The Scatter plot of the position of a collimated gamma source; the abscissa gives the along the strips, deduced from the time difference, and the ordinate is the strip number.

4. IN-BEAM PET SIMULATION STUDIES

The expected performance of the TERA Crystal and MGRPC TOF designs have been studied with the help of the GATE simulation toolkit and compared with a commercial PET scanner GEMINI with the help of the NEMA protocol (V.A. Rosslyn, 2001).
Figure 17 and Figure 18 show simulated full-ring PET systems having as component modules the DOI-CRYSTAL and the MRPC described in the previous sections (Watts, 2014). Number and geometry of the modules are indicated in the figures for the two systems. A detailed study of sensitivity and resolution of the two systems is discussed in the previous reference. As sole example, Figure 19 shows the computed sensitivity to the NEMA source of the MRPC system with 150 µm glass converters for two choices in the number of modules, 60 and 120, and two values of the axial length (30 and 60 cm), as a function of the module's spacing. The full study compares also the performances of full and open-ring geometries for the two options.

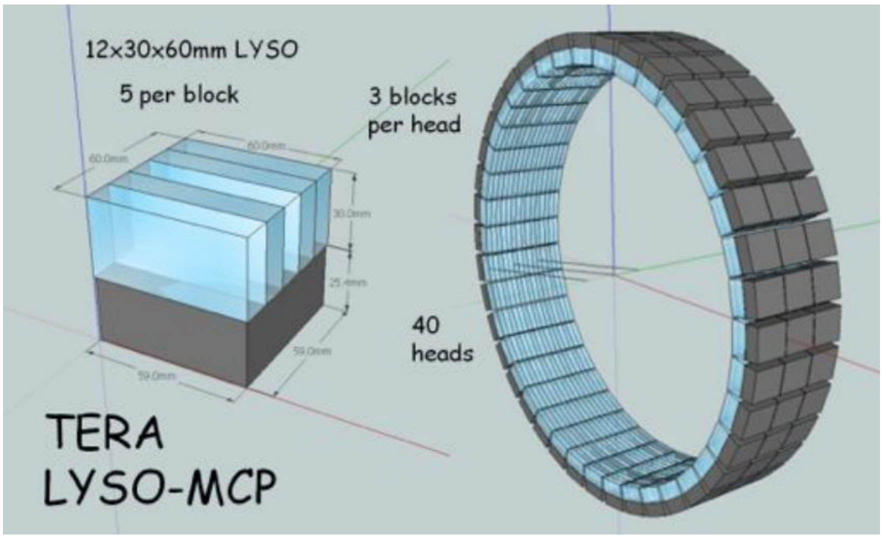

Figure *17*: Full-ring PET scanner based on the TERA DOI-Crystals study.

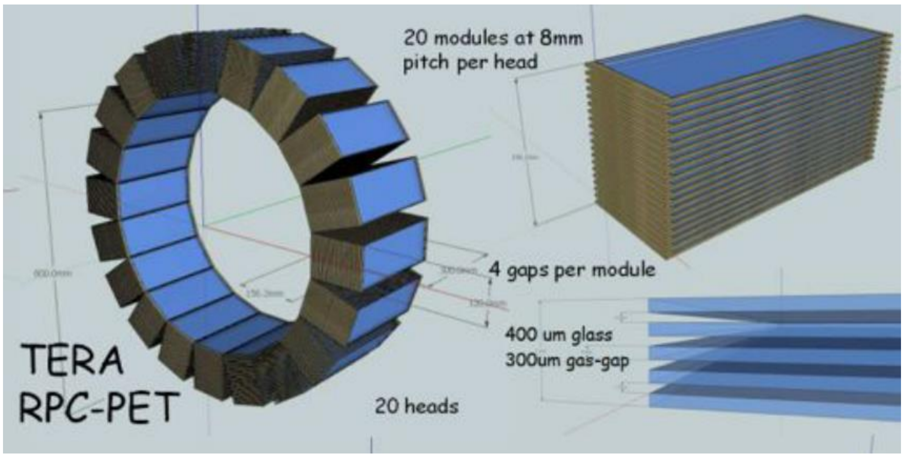

Figure *18*: Full-ring PET scanner based on the TERA MRPC study.

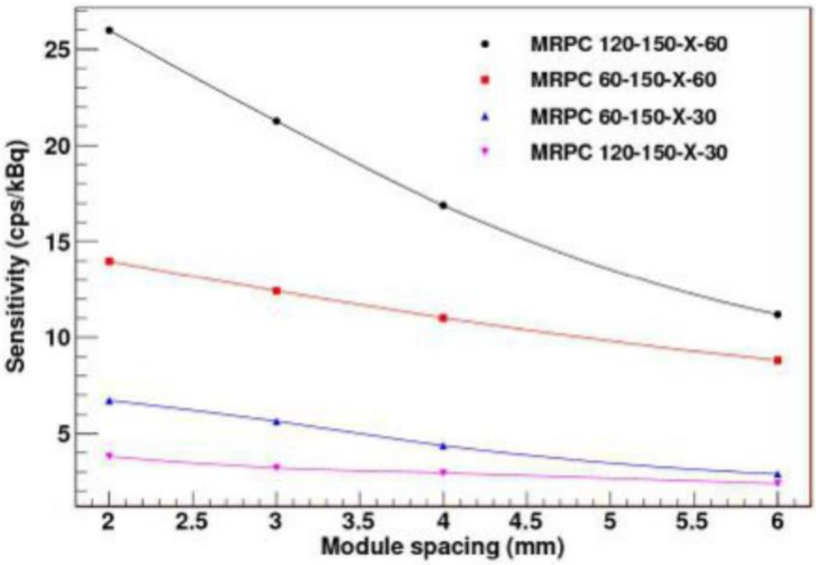

, Figure *19*: MRPC PET sensitivity as a function of module's spacing for 60 and 120 modules and 30 and 60 cm axial length.

5. PROTON RANGE RADIOGRAPHY

The treatment plan with ion beams is determined with an algorithm that takes into account the patient's morphology obtained from X-ray radiography, CAT and IMR scans. The measured density distribution reflects the absorption of X-rays and therefore does not represent the density as seen by the charged particles. This is obtained making use of a table of correction parameters, the so-called Hounsfield scale. While rather sophisticated, the algorithm is prone to errors that can affect the estimate of the optimal dose distribution. A direct measurement of the density with proton beams was proposed long ago (Hanson et al., 1981). Pioneering work was realized in this direction at the Paul-Scherrer-Institute (PSI) (Pemler et al., 1999)(Schneider et al., 2005).
Named Proton Range Radiography (PRR), the system is schematically shown in Figure 20. It includes position-sensitive detectors to record the individual proton tracks and a system to measure the residual energy or range in a fully-absorbing module. For each track, the density-dependent energy loss in the target is deduced as the difference between the beam energy and energy loss in the calorimeter. The energy of the beam has to be higher that the energy for therapy and the intensity is set several orders of magnitude lower to reduce the patient irradiation and the rate requirements on the detectors. Exposures at different angles permit one to realize a tomography image of the target.
The setup developed by AQUA is shown in Figure 21. It includes two fast, two-dimensional tracking detectors based on the Gas Electron Multiplier (GEM) technology, invented by one of the authors (Sauli, 2016), and a stack of thin scintillation counters to determine the residual range. The scheme has been used both for the first prototype, PRR10, with a 10x10 cm^2 acceptance, and the PRR30 with an active area of 30x30 cm^2. With a rate capability of several MHz cm^{-2} and a sub-mm position accuracy, the two GEM detectors provide the incoming particles' trajectory with adequate performance.
Construction and performances of the PRR10 and PRR30 are described in detail in several publications of the AQUA group (Amaldi et al., 2010)(Amaldi et al., 2011)(Bucciantonio et al., 2013b)(Bucciantonio et al., 2013a) and in two Doctoral theses (Watts, 2014)(Bucciantonio, 2015).
A GEM detector module,used for the PRR10, before assembly and mounting of the readout electronics is shown in Figure 22 and is based on the design of the Gas Detectors Development (GDD) group at CERN[2] (Bressan et al., 1999). Figure 23 shows one of the plastic scintillators with a wavelength shifter fibre readout, 30 scintillators, 3 mm thick each, constitute the residual range measurement stack.
The completed PRR10 is shown bare in Figure 24 and with a cover ensuring portability and noise screening in Figure 25.

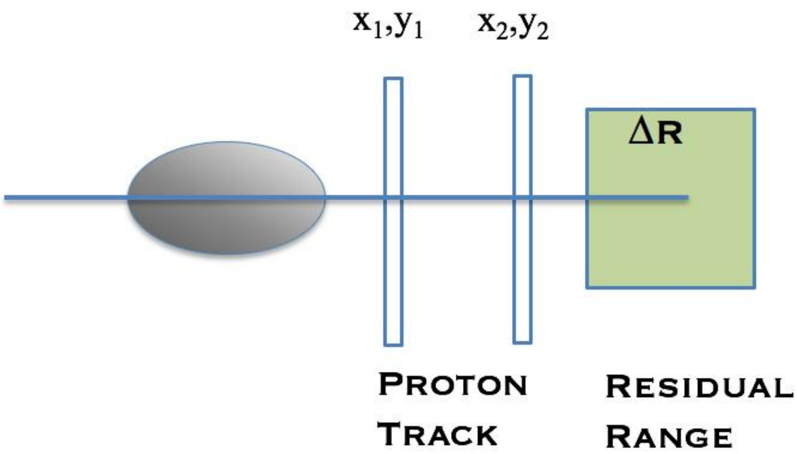

Figure 20: Schematics of the Proton Range Radiography system.

[2] Particular thanks to Leszek Ropelewski and Miranda Van Stenis

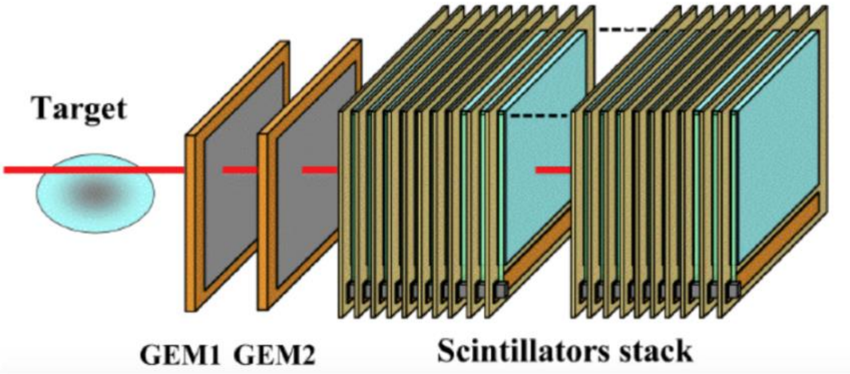

Figure 21: The AQUA Proton Range Radiography setup.

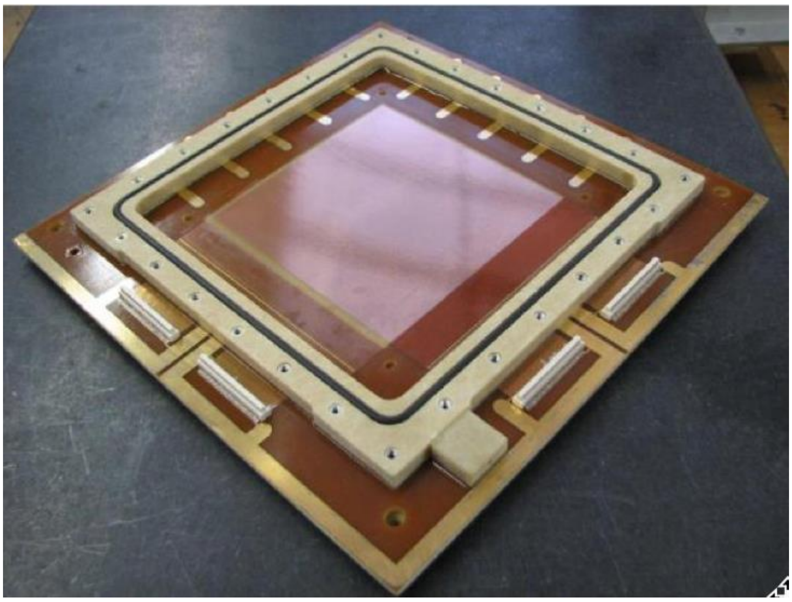

Figure 22: A 10x10 cm^2 active Gas Electron Multiplier module used for the PRR10.

Figure 23: One of the 30 plastic scintillators used to measure the residual proton range.

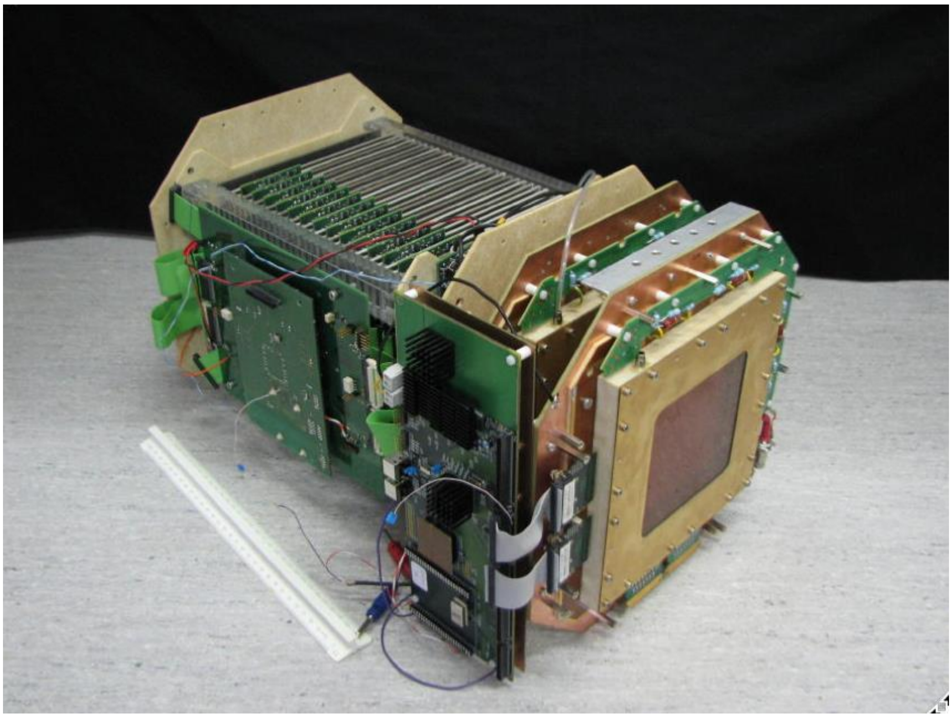

Figure 24: The fully assembled PRR10.

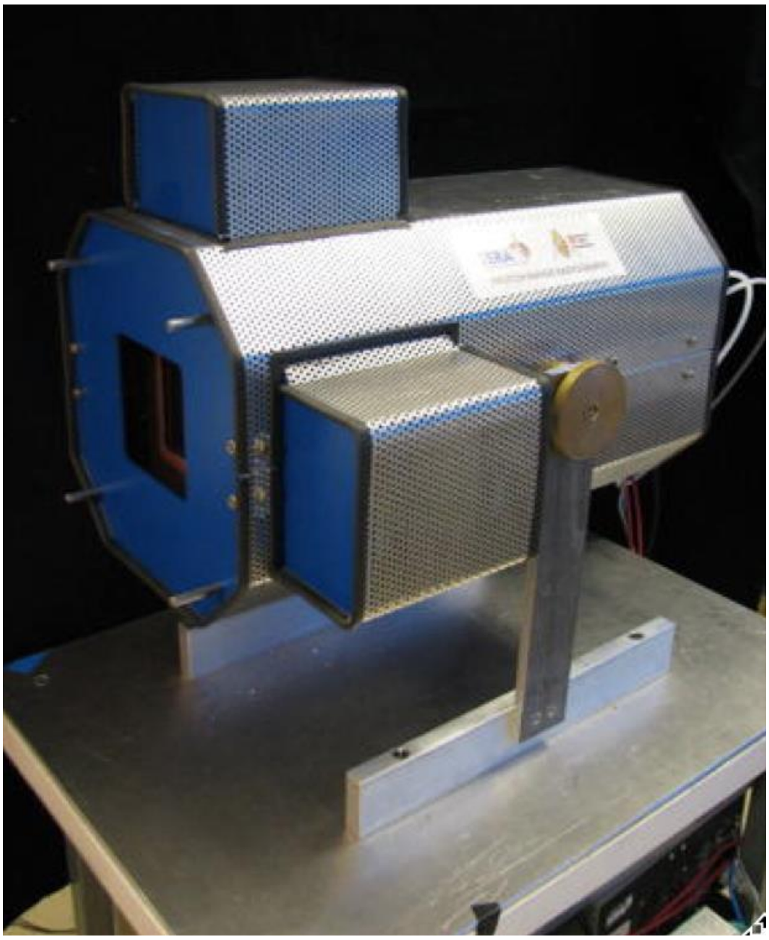

Figure 25: The PRR10 with a boxed cover ensuring portability in a clinical environment.

The performance of the PRR10 has been verified with exposure to a proton beam at the Paul-Scherrer-Institute. Figure 26 shows the differential energy loss profile recorded with the scintillator stack at increasing beam energies. A fit to the distributions provides a residual range resolution of 1.7 mm.
The imaging capability of the detector has been assessed using a 20 mm thick plastic slab as target consisting of patterns of holes with different diameter and depth emulating the density differences (see Figure 27). Figure 28 is the result of the exposure to the proton beam with colors representing the measured density. The smaller holes that are one mm in diameter are well resolved.

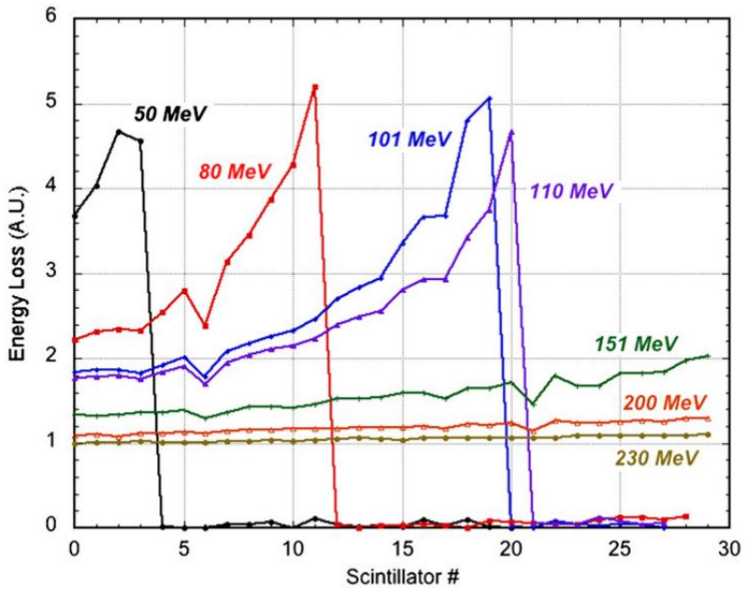

Figure 26: Energy loss as a function of penetration in the scintillator stack at increasing beam energies.

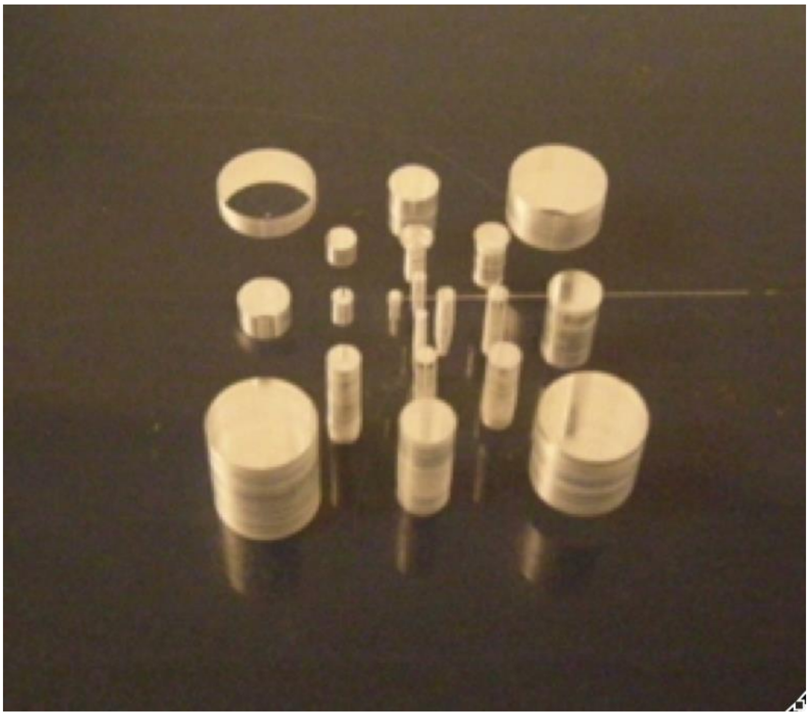

(see Figure *27*: Hole pattern in a 20 mm thick plastic slab; holes vary in diameter from 1 to 10 mm, and are drilled to a depth of 5 to 10 mm.

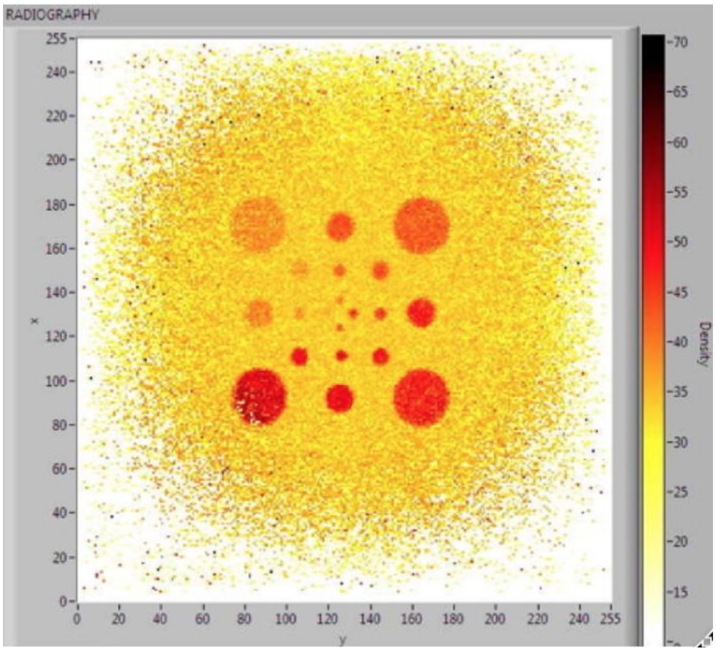

). Figure *28*: Proton Range Radiography at 100 MeV of the target shown in the previous figure. The space and density resolutions are better than 1 mm and 2%, respectively.

While the PRR10 operated according to the specifications, its small size and limited data acquisition rate (below 100 kHz) restrained its use for clinical applications. It was therefore decided to build a larger module, the PRR30, with a 30x30 cm^2 active area and improved electronics. Larger GEM trackers, based on CERN's COMPASS experiment design (Altunbas et al., 2002) were built[3] as well as a stack of 47 plastic scintillators, extending the energy range coverage up to 230 MeV. Figure 29 shows Jerome Samarati working on one of the large GEM modules. Figure 30 shows the completed detectors. The fully assembled PRR30 is shown in Figure 31.

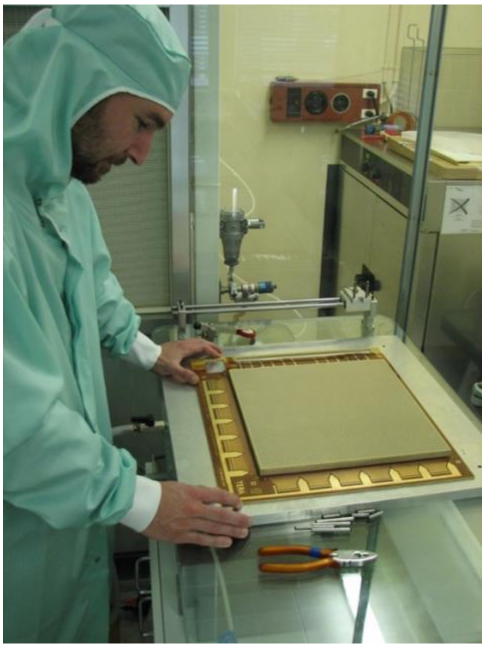

Figure 29: Jerome Samarati assemblying one of the large GEM detectors.

[3] The help of CERN's GDD group, and in particular Leszek Ropelewski and Miranda van Stenis is here acknowledged.

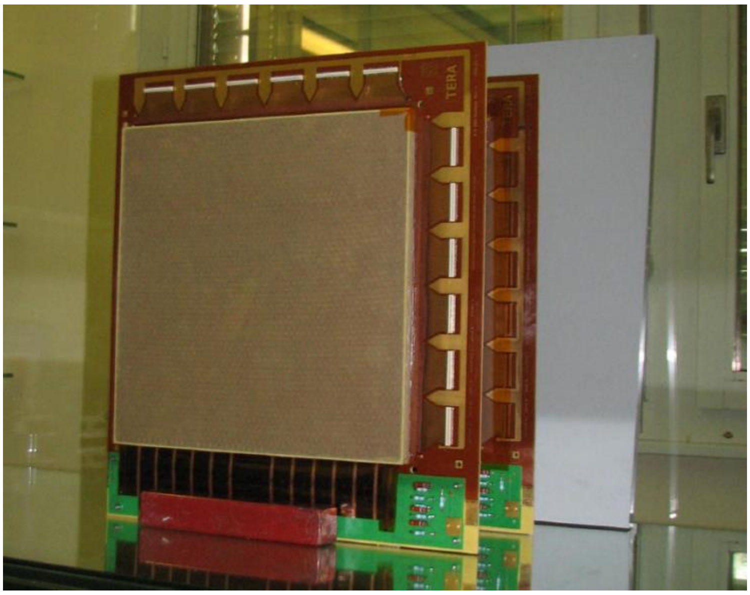

. Figure 30: The two GEM trackers for the PRR30.

Figure 31: The PRR30, with 30x30 cm^2 active imaging area and a 47 scintillators stack.

The module was tested at PSI, recording with the design resolution the penetration depth at energies between 70 and 230 MeV (see Figure 32).
Due to lack of support, however, the group could not pursue the development of the PRR30 which was transferred to a group at the Vienna Technical Institute in view of an application at the MEDAUSTRON therapy center.

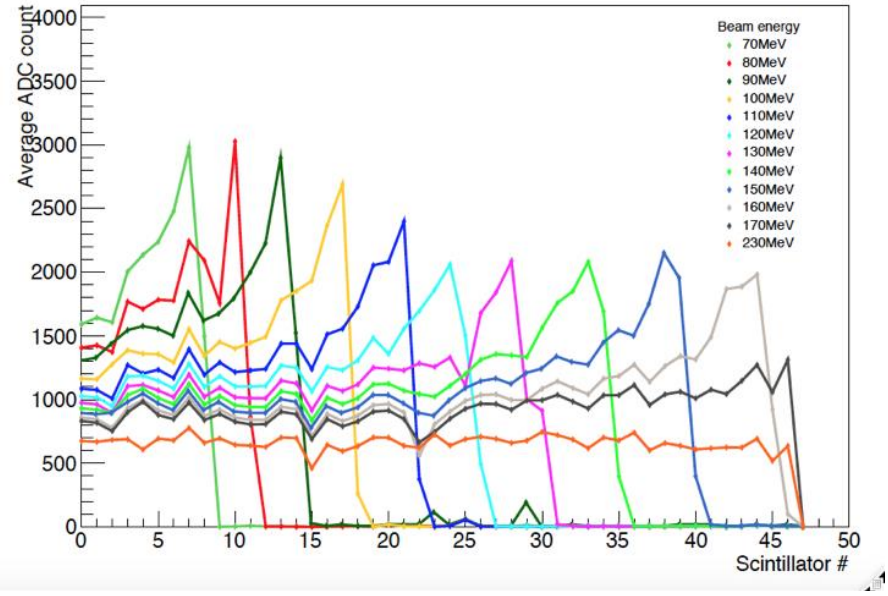

(see Figure 32: Differential energy loss as a function of penetration in the 47-scintillator stack.

6. PROMPT GAMMA MONITOR (PGM)

Of all radiation yields, the best candidates to provide an image of the deposited dose are the prompt gammas emitted by the interaction of ion beams with the body. On one hand, the energy required for their production (MeV) is small enough to result in copious emission down to the end of the absorption range. On the other hand, MeV photons have modest absorption and scatter in soft tissue, preserving the image of the absorbed range.
The computed dependence of the energy loss in the Bragg peak and the secondary radiation yield for protons is shown in Figure 33. Thehe photon yield follows well the energy loss intensity in the Bragg peak. An example of the energy spectrum of prompt photons for several proton energies is given in Figure 34.
While it is relatively easy to detect photons in the MeV range, so is the probability to detect neutrons in the same energy range. Due to their scattering by nuclear interactions in the target, neutrons do not provide a valid image of the dose and constitute a severe background in the detection of prompt gammas for this purpose.

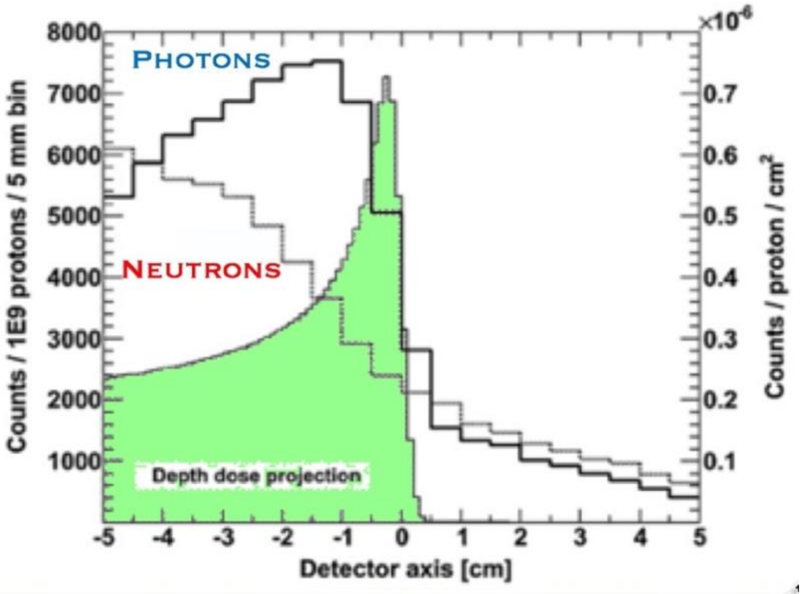

Figure 33: Differential energy loss, photons and neutrons yields for protons in a target near the Bragg peak.

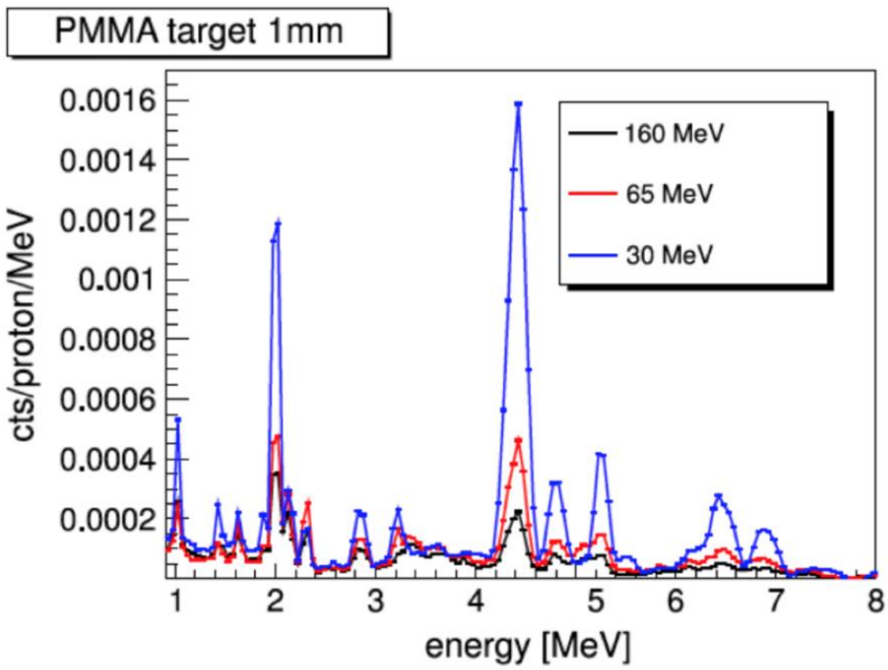

Figure 34: Energy spectra of prompt gammas emitted by stopping protons at three energy values.

After analysis of various methods apt at reducing the neutron sensitivity in crystal-base photon detectors, a possible solution was investigated taking into account the different interaction processes of neutrons and MeV gammas (see Figure 35). While the nuclear interactions of neutrons result in a local release of energy, photons interacting via electromagnetic processes (photoelectric, Compton) initiate an electromagnetic shower several cm long. Splitting the detector in two layers and requiring a coincidence between the sections is expected to reduce the neutron background. This has been confirmed by the simulation, as described below.

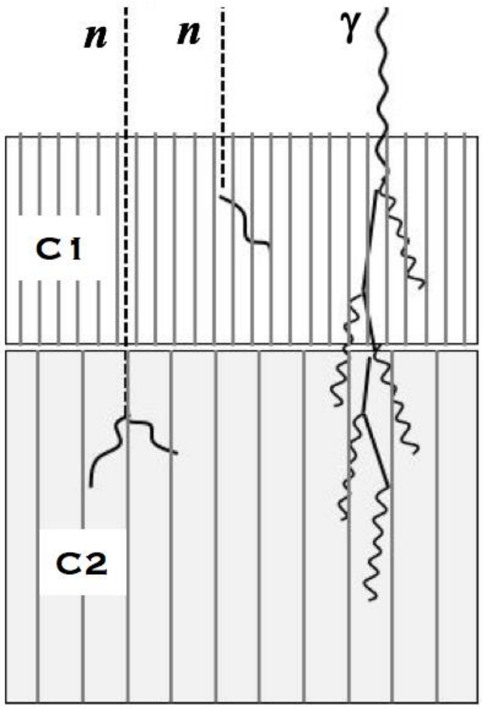

Figure 35: Layman description of neutron and gamma ray interactions in a double-layer detector.

The response of the double-layer scintillating crystal detector has been simulated using a GEANT4 toolkit specifically developed for hadrontherapy applications (G.A.P. Cimone et al., n.d.). Optimization of the geometry as a function of the layers' thickness, of the application of suitable cuts in the energy deposited in each layer, of the transverse size of the detected scintillation profiles and of the total energy results in an estimated improvement in the value of the ratio of prompt gammas to neutrons by a factor of five, deemed sufficient for imaging [4].
The basic design of the PGM (see Figure 36) has two segmented crystal scintillators layers named "interaction" and "energy" according to their function. The scintillators in the first layer provide the position of the gamma conversion and have, therefore, a size corresponding to the desired localization accuracy. The second layer, with larger crystals, is thick enough to absorb all the energy of the shower. Detection and localization of the scintillation is performed with silicon photomultiplier arrays or a multi-anode PM as described in Chapter 2. A possible more advanced design, Figure 37, uses sets of parallel wavelength shifter bars to provide both the energy release and the position of the conversion.
The AQUA Prompt Gamma Monitor project has been transferred to the TERA offspring company EBAMed, based in Geneva. It is covered by an international patent (Garonna and Sauli, 2020).

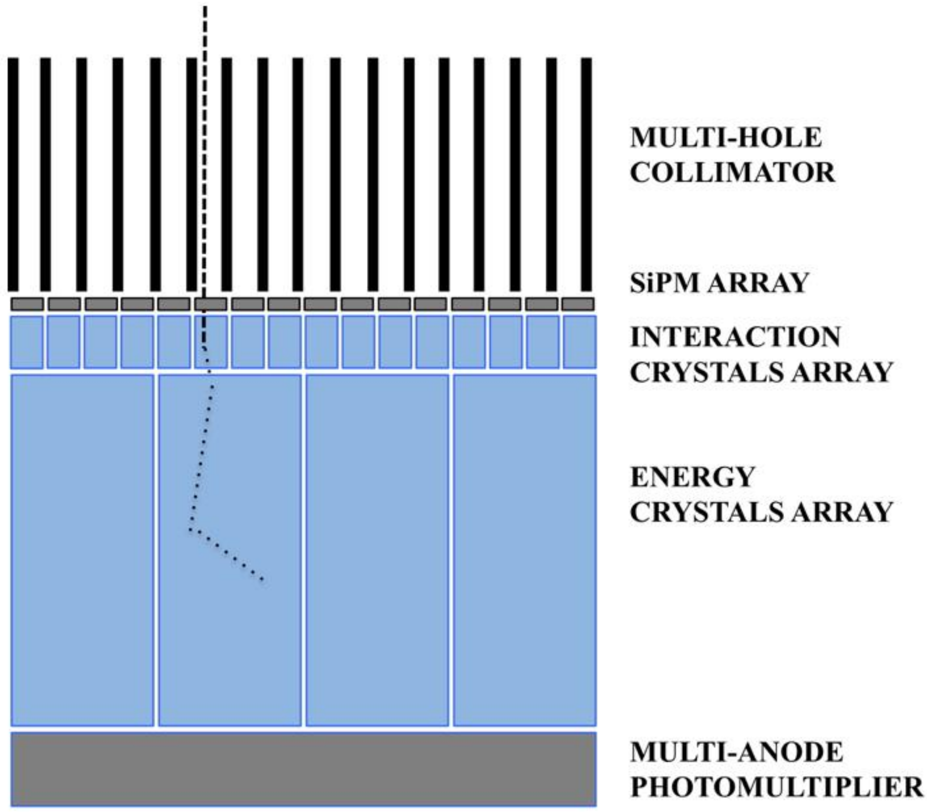

(see Figure *36*: A dual-layer PGM with collimator and readout of the scintillation light.

[4] Simulations by C. Cuccagna and E. Ripiccini

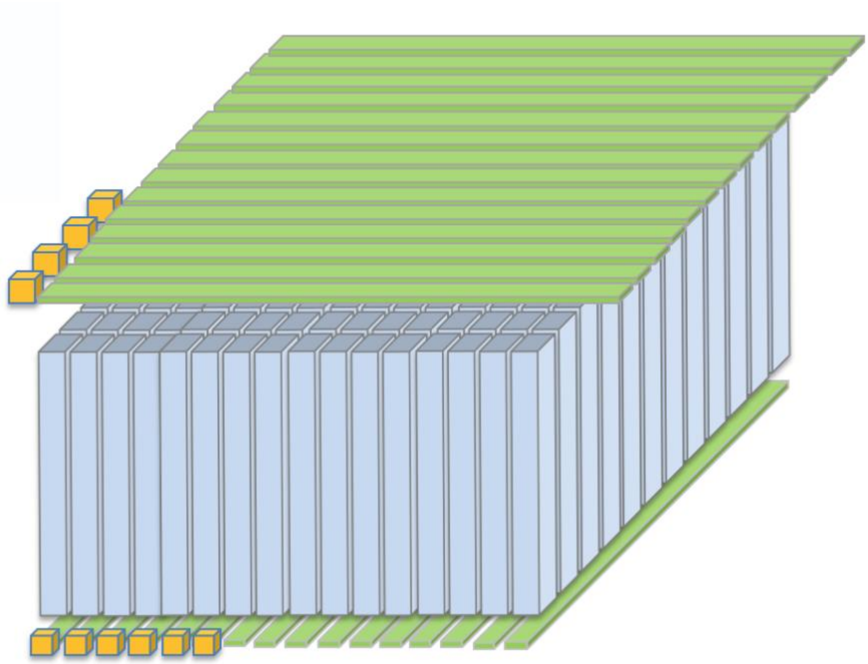

Figure 37: Proposed implementation of a PGM layer with WLS bars and silicon PM readout providing position and energy loss of the conversion.

7. PRINCIPAL TERA-AQUA COLLABORATORS

CERN:
Ugo Amaldi
Fabio Sauli
Martina Bucciantonio
Sarolta Iliescu
David Watts
Robert Kieffer
Giacomo Borghi
Jerome Samarati
Nail Malakhov
Andrea Bianchi
Mattia Fontana
Caterina Cuccagna

BERN UNIVERSITY:
Saverio Braccini

PAUL-SCHERRER-INSTITUTE:
Wojtek Hajdas

CENTRO NAZIONALE DI ADROTERAPIA ONCOLOGICA (CNAO):
Marco Donetti
Marco Pullia

NATIONAL CENTRAL UNIVERSIT TAIWAN:
Apollo Go
Y.H. Chang

REFERENCES

Akindinov, A.N., Alici, A., Anselmo, F., Antonioli, P., Basile, M., Al, E., 2004. Latest results on the performance of the multigap resistive plate chamber used for the ALICE TOF. Nucl. Instr. Meth. Phys. Res. A 533, 74.

Altunbas, C., Capeans, M., Dehmelt, K., Ehlers, J., Friedrich, J., Konorov, I., Gandi, A., Kappler, S., Ketzer, B., De Oliveira, R., Paul, S., Placci, A., Ropelewski, L., Sauli, F., Simon, F., Van Stenis, M., 2002. Construction, test and commissioning of the triple-gem tracking detector for COMPASS. Nucl. Instr. Meth. Phys. Res. A 490, 177–203.

Amaldi, U., Bianchi, A., Chang, Y.-H., Go, A., Hajdas, W., Malakhov, N., Samarati, J., Sauli, F., Watts, D., 2011. Construction, test and operation of a proton range radiography system radiography system. Nucl. Instr. Meth. Phys. Res. A 629, 337–344. https://doi.org/10.1016/j.nima.2010.11.096

Amaldi, U., Borghi, G., Bucciantonio, M., Kieffer, R., Samarati, J., Sauli, F., Watts, D., 2015. Development of TOF-PET detectors based on the Multi-Gap Resistive Plate Chambers. Nucl. Instr. Meth. Phys. Res. A 778, 85–91. https://doi.org/10.1016/j.nima.2015.01.018

Amaldi, U., Hajdas, W., Iliescu, S., Malakhov, N., Samarati, J., Sauli, F., Watts, D., 2010. Advanced Quality Assurance for CNAO. Nucl. Instr. Meth. Phys. Res. A 617, 248–249. https://doi.org/10.1016/j.nima.2009.06.087

Anghinolfi, F., Jarron, P., Martemiyanov, A.N., Usenko, E., Wenninger, H., Williams, M.S.C., Zichichi, A., 2004. NINO: an ultra-fast and low-power front-end amplifier/discriminator ASIC designed for the multigap resistive plate chamber. Nucl. Instr. and Meth. A533, 183.

Bressan, A., Labbé, J.C., Pagano, P., Ropelewski, L., Sauli, F., 1999. Beam tests of the gas electron multiplier. Nucl. Instr. Meth. Phys. Res. A 425, 262–276. https://doi.org/10.1016/S0168-9002(98)01406-5

Bucciantonio, M., 2015. Development of an advanced Proton Range Radiography system for hadrontherapy. PhD BERN Univ.

Bucciantonio, M., Amaldi, U., Kieffer, R., Malakhov, N., Sauli, F., Watts, D., 2013a. Fast readout of GEM detectors for medical imaging. Nucl. Instr. Meth. Phys. Res. A 718, 160–163. https://doi.org/10.1016/j.nima.2012.10.046

Bucciantonio, M., Amaldi, U., Kieffer, R., Sauli, F., Watts, D., 2013b. Development of a fast proton range radiography system for quality assurance in hadrontherapy. Nucl. Instr. Meth. Phys. Res. A 732, 564–567. https://doi.org/10.1016/j.nima.2013.05.110

Cerron-Zeballos, E., Crotty, I., Hatzifotiadou, D., Valverde, J.L., Williams, M.C.S., 1996. A new type of resistive plate chamber: The multigap RPC. Nucl. Instr. and Meth. A 374, 132.

Diblen, F., Rohling, H., Torres-Espallardo, I., Solevi, P., Gillam, J., Watts, D., Espana, S., Vandenberghe, S., Fiedler, F., Rafecas, M., 2012. Comparison study of RPC and crystal based PET systems for hadron therapy monitoring. IEEE Nucl. Sci. Symp. Conf. Rec. 2212–2217. https://doi.org/10.1109/NSSMIC.2012.6551504

Dosanjh, M., 2017. From Particle Physics to Medical Applictions. IOP Sci.

ENLIGHT [WWW Document], 2020. URL https://enlight.web.cern.ch/

G.A.P. Cimone, L. Pandola, et al., n.d. Advanced Examples Hadrontherapy Geant4 [WWW Document]. URL https://twiki.cern.ch/twiki/bin/view/Geant4/AdvancedExamplesHadrontherapy (accessed 10.11.22).

Garonna, A., Sauli, F., 2020. Dual Layer Prompt Gamma Monitor. WO 2020/0751068 A2.

Hanson, K.M., Bradbury, J.N., Cannon, T.M., Hutson, R.L., Laubacher, B., Macek, R.J., Paciotti, M.A., Taylorf, C.A., 1981. Computed tomography using proton energy loss. Phys Med Biol 26, 965–983.

Pemler, P., Besserer, J., De Boer, J., Dellert, M., Gahn, C., Moosburger, M., Schneider, U., Pedroni, E., Stak, H., 1999. A detector system for proton radiography on the gantry of the Paul-Scherrer-Institute. Nucl. Instr. Meth. Phys. Res. A 432, 483–495.

Sauli, F., 2016. The gas electron multiplier (GEM): Operating principles and applications. Nucl. Instr. Meth. Phys. Res. A 805, 2–24. https://doi.org/10.1016/j.nima.2015.07.060

Schneider, U., Pemler, P., Besserer, J., Pedroni, E., Lomax, A., Kaser-Hotz, B., 2005. Patient specific optimization of the relation between CT-Hounsfield units and proton stopping power with

proton radiography. Med. Phys. 32, 195.
Solevi, P., 2007. Study of an in-beam PET system for CNAO, the National Centre for Oncological Hadrontherapy. Univ. Milano.
V.A. Rosslyn, 2001. NEMA Standard Publication NU2-2001.
Watts, D., Borghi, G., Sauli, F., Amaldi, U., 2013. The use of multi-gap resistive plate chambers for in-beam PET in proton and carbon ion therapy. J. Radiat. Res. 54 Suppl 1, 1136. https://doi.org/10.1093/jrr/rrt042
Watts, D.A., 2014. Detectors for Quality Assurance in Hadrontherapy. PhD Univ. Barcelona.